sustainability

MDPI

Article

Barrier Longevity of NaCl-Laden Soil against Subterranean Termites in an Earth Embankment

Ying Li [1] and Dong-Zi Pan [2,*]

[1] College of Geomatics and Municipal Engineering, Zhejiang University of Water Resources and Electric Power, Hangzhou 310018, China; liying@zjweu.edu.cn
[2] Zhejiang Institute of Hydraulics and Estuary, Hangzhou 310012, China
* Correspondence: pandz@zjwater.gov.cn; Tel.: +86-571-8643-8014

Abstract: Subterranean termite-induced damage to earth embankments in agricultural systems occurs globally. NaCl-laden soil barriers (NLSBs) are an environmentally sustainable termite control method, and have exhibited good potential in preventing termite-related tunneling damage in Zhejiang Province, China. The persistence of the NaCl concentration in NLSBs is a key characteristic for the long-term prevention of subterranean termite infestations. This study is a scientific attempt to estimate the field efficacy and barrier longevity of NLSBs in reservoir embankments based on the Richards equation and the convection–dispersion equation using HYDRUS (2D/3D). The observed and simulated NaCl concentrations at the end of a 1915-day simulation were compared. The results indicated that the proposed model performed well and can effectively characterize the water flow and salt transport in NLSBs. The salt desalination rate of the NLSB in the upstream slope was higher than that in the downstream slope, both of which were significantly higher than that at the embankment axis. Regardless of the type of embankment (homogeneous or core-wall), the barrier longevity of NaCl-laden soil against subterranean termites can reach 50 years with an optimized NaCl/soil ratio in different parts of the embankment.

Keywords: termite control; earth embankment; HYDRUS (2D/3D); modelling

Citation: Li, Y.; Pan, D.-Z. Barrier Longevity of NaCl-Laden Soil against Subterranean Termites in an Earth Embankment. *Sustainability* **2021**, *13*, 13360. https://doi.org/10.3390/su132313360

Academic Editor: Clara Celauro

Received: 5 November 2021
Accepted: 28 November 2021
Published: 2 December 2021

1. Introduction

Numerous irrigation reservoirs have been built in the paddy farming regions of southern China to accommodate excess rainwater during the rainy season. Most of these reservoirs have earth embankments with a high clay content, an appropriate soil pH value, and suitable particle properties that are attractive to termites that build nests and tunnels inside the reservoir embankment [1–3]. These internal tunnel networks can weaken the embankment structure, causing leakage, erosion, and collapse, and resulting in significant economic losses [4–8]. According to one survey, 90% of all of the reservoir embankments and river dams in the 14 provinces in southern China that were at least 15 years old exhibited some level of subterranean termite-induced damage [9]. In recent years termite-induced damage to earth embankments has increased owing to the influence of climate change [10].

Subterranean termite-induced damage to earth embankments and dams is a global problem. A total of 64 species of termites from four families (*Kalotermitidae*, *Termopsidae*, *Rhinotermitidae* and *Termitidae*) have invaded various dam sites across Vietnam [11,12]. Similar termite damage was identified on dikes along the Mississippi River in New Orleans, USA, which were subsequently destroyed by Hurricane Katrina [13,14]. The presence of termites in embankments and dams has also been reported in India [15,16], Nigeria [17] and Thailand [18]. Although many species of termites attack dams and reservoirs, subterranean termites from the the *Odontotermes* and *Macrotermes* genera pose the most significant threat [19,20]. More than 90% of the dams and reservoirs in southern China are damaged by *Odontotermes formosanus* (Shiraki) and *Macrotermes barneyi* (Light) [21]. Similarly, *Odontotermes hainanensis* (Light) causes the most damage to dams in northern Vietnam [12]. The traditional methods of preventing subterranean termite infestations in China include digging out termite colonies or using termiticides [4]. The former requires a significant amount of time and labor, and the latter is harmful to the environment. The bait method has also been employed recently; however, a small amount of insect toxicants is still required. Termite control using non-toxic physical barriers is an environmentally friendly method that uses non-chemical materials to prevent termite entry and tunneling damage in agricultural systems and commercial buildings [22].

With over 20 years of popularization and application in Zhejiang Province, China, NaCl-laden soil barriers (NLSBs) have proven to be a promising field technique to control subterranean termites in earth embankments [2,23,24]. NLSBs are an indigenous approach that utilizes NaCl as a mixing agent in cohesive soils, with the aim of preventing subterranean termite penetration and damage to earth embankments and dams. Both the sodium and chloride ions contribute to the inhibition in metabolizing cellulose, which might be sufficient to starve termites, thereby killing them [25]. Moreover, as a hygroscopic material, NaCl has the ability to draw off moisture as it comes into contact with a moisture-laden body. If termites persist in advancing through the NLSB, they will tend to die of dehydration [26]. As NaCl is nonvolatile and robust as an inert particle, and is used only in small amounts (NaCl/soil ratio of 0.8%) [23], NLSBs are considered to be an environmentally sustainable control method. Adequate NaCl concentration in the NLSB is a key method for the long-term prevention of subterranean termite infestations. The failure of NLSB-based treatments is often due to environmental factors, such as repeated water level cycles, saturated hydraulic conductivity of the soil matrix and rainfall infiltration [24].

Cyclodienes, especially chlordane, are stable and extremely effective in soil and have been used to protect structures from subterranean termites for decades [27]. Under a global treaty known as the Stockholm Convention, chlordane and mirex, which were once widely used as termite control agents, have been banned in most countries around the world [28]. Currently, most termiticides are more expensive and less persistent than cyclodienes [29]. The standard measure for acceptable performance in the United States is that termiticides must prevent termites from penetrating 90% of the barrier for at least five years [30]. Treatment failures and concerns about increased pesticide use have led to a renewed interest in developing alternative subterranean termite control methods [31]. NLSBs are an indigenous practice that must be properly evaluated to determine their field efficacy and longevity.

Owing to the lack of a careful scientific evaluation of the long-term persistence of NLSBs against subterranean termites in earth embankments, an accurate assessment of their relative potential is difficult. Some solutes in an NLSB are transported over time by moving water through advection and dispersion. Variations in soil properties such as hydraulic conductivity, clay and organic matter content and water content can also influence the groundwater and salt transportation characteristics of NLSBs in embankments [24]. Numerous field and laboratory methods have been applied to characterize the transport of water and solutes in soil and to monitor the soil moisture content. Computer models for characterizing mass transfer processes in soil have also been developed [32–34]. Numerical simulations using calibrated models can also evaluate soil water and solute dynamics over a sufficiently long duration.

The HYDRUS (2D/3D) model [35] has been widely used in the analysis of water, heat and solute transport in variably saturated porous media in agricultural systems [36–40]. In this study, we developed a simple NLSB treatment for a post-construction earth embankment using casing-wells to backfill NaCl-laden soil, which acts as a barrier against subterranean termites. The variation in the NaCl concentration in the NLSB was analyzed through field measurements in the Longxi Reservoir (LR) in Yuhuan, Zhejiang Province, China. Subsequently, considering homogeneous and core-wall embankments, the barrier longevity of the NLSB was estimated based on the extent of salt desalination using the HYDRUS (2D/3D) model. Finally, we discuss the future research directions of this approach.

2. Materials and Methods

2.1. Site Specification

The LR is a small reservoir that is primarily used to supply water and is integrated with irrigation, flood control and drainage systems. It is located in Yuhuan, Zhejiang Province, China (Figure 1). The reservoir basin is dominated by hills, with a rainwater collection area of 5.1 km^2, a main river course of 2.95 km and an average gradient of 2.6%. Currently, the normal storage capacity is 2.71 million m^3, with a total storage capacity of 3.31 million m^3. The local climate is subtropical marine, with an average annual rainfall of 1350 mm, of which approximately 1000 mm is distributed during March–September.

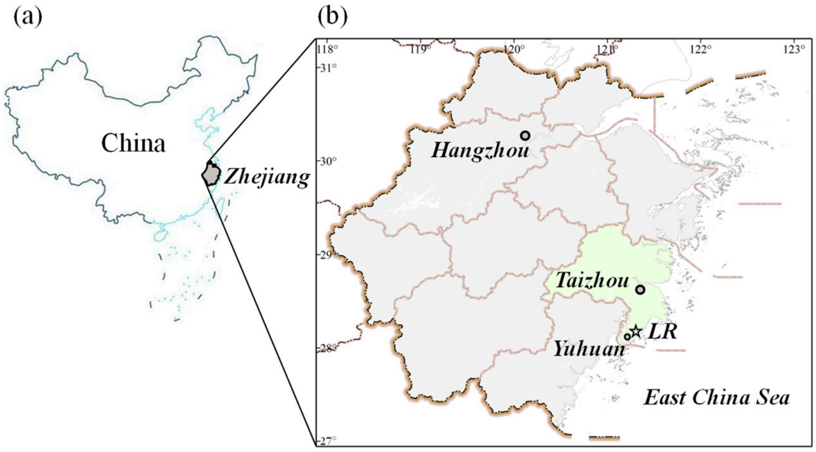

Figure 1. Study area: (**a**) Zhejiang province in China and (**b**) Location of the Longxi Reservoir (LR).

2.2. Field Treatment

The construction process of a NLSB using casing-wells to backfill NaCl-laden soil primarily consists of five steps—drilling arrangement, well making, soil borrowing, soil/NaCl mixing and backfilling. The specific construction process is shown in Figure 2, and the primary design considerations are as follows:

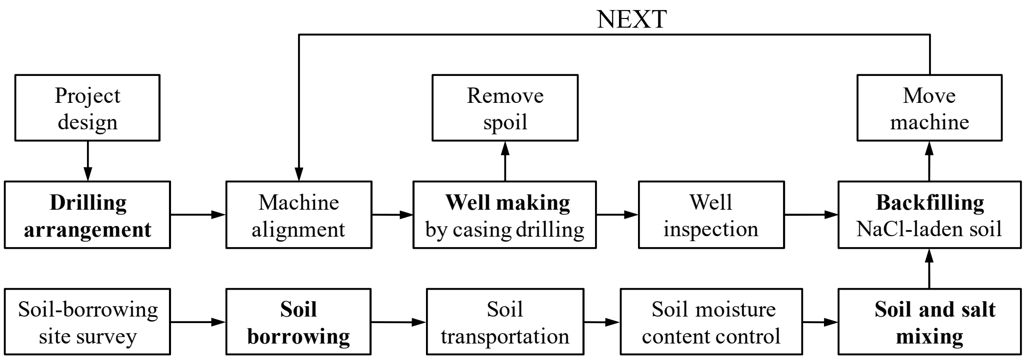

Figure 2. The specific construction process of NLSB field treatment.

Step 1. Drilling arrangement of casing well. Considering the reduction in the phreatic line, the wells are arranged on the dam axis or the upstream side of the dam crest parallel to the dam axis. The required thickness of the clay cut-off wall for casing backfilling is determined based on the seepage gradient. Earth embankments with a height of less than 15 m are designed with a single row of casing wells, whereas two or three rows of casing wells are used for those with a height of more than 15 m.

Step 2: Well making by casing drilling. First, two main wells (Nos. 1 and 2 in Figure 3) are drilled, backfilled and tamped. Subsequently, a casing well (No. 3) is drilled between the two main wells. This procedure is repeated until all the wells are drilled. The main wells and casing wells are embedded to a depth of 1–2 m in the underlying soil layer, and penetrate the impermeable layer if necessary.

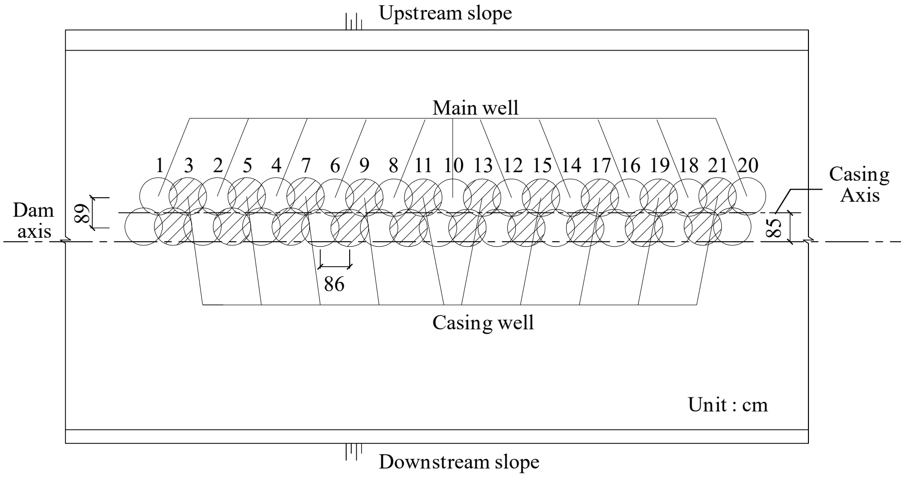

Figure 3. Typical construction diagram of casing wells.

Step 3: Soil borrowing. The backfill soil is clay loam, with a suitable water content based on the design requirements. The water content is controlled through tedding or watering.

Step 4: Soil NaCl mixing. The salt content is calculated based on the dry density of the soil to ensure a NaCl/soil ratio of 0.8% (at least 0.2%) in the NLSB. The soil and NaCl are mixed evenly.

Step 5: Backfilling and tamping. After the wells are made, they must be immediately and continuously backfilled and compacted in layers. The thickness of each layered backfill is approximately 0.3–0.5 m, and care must be taken to ensure that no water is present at the bottom of the well during backfilling. The construction parameters, including the optimal paving thickness, falling distance and tamping duration, are determined through field experiments.

2.3. Soil Characterization

To ensure the safe operation of the reservoir dam in the future, reinforcement and reconstruction projects were performed in 2009, and the NLSB technique was used to prevent termite infestations. Laboratory tests were performed on undisturbed soil samples collected from various locations along the embankment before and after the project construction. The samples were identified and classified through index property tests to determine the soil texture and bulk density. The permeability of the soil was evaluated through a variable head permeability test. The concentration of soluble salt in the soil was determined by measuring the conductivity of the soil water extract.

2.4. Numerical Model

2.4.1. Governing Equations

Considering the isothermal uniform Darcy flow in variable saturated rigid porous media and ignoring the influence of the gas phase in the liquid phase flow, the modified Richards equation can be used to describe soil water movement in the HYDRUS (2D/3D) model [41].

$$\frac{\partial \theta}{\partial t} = \nabla \cdot (K\nabla h + K\nabla z) - S \quad (1)$$

where t is the time [T]; h is the water pressure head [L]; θ is the volumetric water content [L^3L^{-3}]; $K(\theta)$ is the unsaturated hydraulic conductivity function [LT^{-1}]; ∇ is a vector differential operator [L^{-1}]; z is a Cartesian coordinate [L]; S is the general sink term [$L^3L^{-3}T^{-1}$], which is not considered herein.

The van Genuchten–Mualem formula can be used to estimate the water retention properties and hydraulic conductivity of the soil [42]:

$$\theta(h) = \left\{ \begin{array}{c} \theta_r + \frac{\theta_s - \theta_r}{\left[1+|\alpha h|^n\right]^m} \;\; ; \quad h < 0 \\ \theta_s \;\; ; \quad h \geq 0 \end{array} \right\} \tag{2a}$$

$$K(\theta) = K_s S_e^l \left[1 - (1 - S_e^{1/m})^m\right]^2 \tag{2b}$$

where θ_s and θ_r are the saturated and residual water contents [L^3L^{-3}], respectively; K_s is the saturated hydraulic conductivity [LT^{-1}]; $S_e = (\theta - \theta_r)/(\theta_r - \theta_s)$ is the effective saturation; α is the inverse of the air-entry suction value [L^{-1}]; n is the pore-size distribution index; l and m are empirical parameters related to the pore-connectivity and pore size distribution, respectively. Herein, l = 0.5 and $m = 1 - (1/n)$, ($n > 1$).

As a conservative solute, NaCl transport is expressed using the advective–dispersive equation:

$$\frac{\partial \theta c}{\partial t} = -\nabla \cdot (\mathbf{q}c - \theta\,\mathbf{D}\nabla c) - S_c \tag{3}$$

where c is the solute concentration [ML^{-3}]; q is the volumetric water flux density vector [$L^3L^{-2}T^{-1}$]; $\mathbf{D}$ is the dispersion tensor [L^2T^{-1}]; S_c is the sink term, which is not considered herein. The components of $\mathbf{D}$ are [43]:

$$\theta\,\mathbf{D} = \theta D_{ij} = D_T|\mathbf{q}|\delta_{ij} + (D_L - D_T)\frac{q_i q_j}{|\mathbf{q}|} + \theta D_d \tau \delta_{ij} \tag{4}$$

where D_{ij} is a component of the dispersion tensor [L^2T^{-1}]; D_L and D_T are the longitudinal and transversal dispersivity [L], respectively; D_d is the molecular diffusion coefficient in free water [L^2T^{-1}]; q_k ($k = i, j$) is the k-component of $\mathbf{q}$ [$L^3L^{-2}T^{-1}$]; τ is the tortuosity factor; δ_{ij} is the Kronecker delta function.

2.4.2. Model Domain, Boundary, and Initial Conditions

The main dam of the LR is a core-wall embankment comprising a combination of permeable and relatively impermeable materials in the embankment cross-section (Figure 4a). Table 1 lists the parameter values used in the model, which were obtained from either laboratory tests or the existing literature. The size of the model domain is equal to the actual size of the LR embankment. The embankment has a crest width of 5 m, bottom width of 115 m and height of 25 m.

The initial conditions of the measured soil moisture were used in the model. A time-variable pressure head boundary condition was defined at the upstream slope of the embankment (Figure 5). The water levels along the discharge trench at the downstream slope remained constant at 1 m during the simulation. The seepage face boundary conditions were considered on the surface of the toe drain. No flux boundary conditions were applied on the remainder of the domain surface. The region was discretized into two-dimensional triangular elements using the Meshgen tool in the HYDRUS software package. The resulting finite element method (FEM) mesh contained approximately 9000 nodes and 18,000 triangular elements. The FEM mesh and boundary conditions of the earth embankment are shown in Figure 4b.

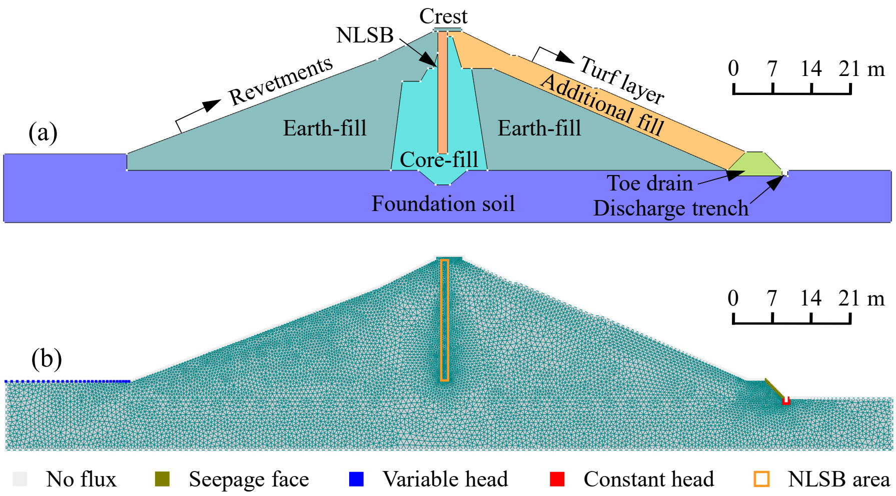

Figure 4. (**a**) Model geometry and (**b**) FEM mesh and boundary conditions of the LR used in the HYDRUS (2D/3D) simulations.

Table 1. Selected soil and water characteristic parameters of the main dam of the LR.

Parameter	* EF	CF	FS	NLSB	TD	AF
Residual water content, θ_r [m^3m^{-3}]	0.034	0.07	0.02	0.07	0.015	0.045
Saturated water content, θ_s [m^3m^{-3}]	0.46	0.37	0.42	0.37	0.41	0.43
Empirical parameter, α [m^{-1}]	1.6	0.5	0.3	0.5	1.5	14.5
Empirical parameter, n	1.37	1.09	1.3	1.09	2.68	2.68
Empirical parameter, l	0.5	0.5	0.5	0.5	0.5	0.5
Saturated hydraulic conductivity, K_s [md^{-1}]	0.026	1.08×10^{-3}	5.4×10^{-3}	1.08×10^{-3}	108	7.128

* EF: earth-fill, CF: core-fill, FS: foundation soil, NLSB: NaCl-laden soil barrier, TD: toe drain, AF: additional fill.

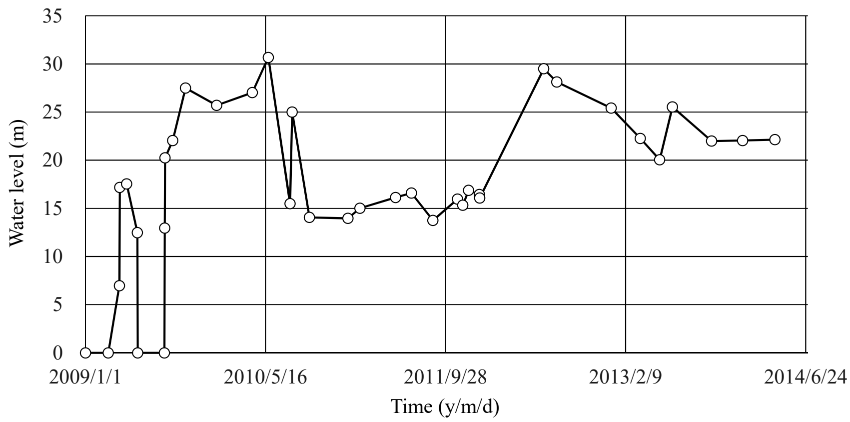

Figure 5. Temporal variation in the pressure head boundary condition along the upstream slope during the simulation.

The concentration of NaCl in the solid phase of the NLSB was 2 g/kg at the start of the simulation. The total simulation time was 1915 days. Primarily, the change in the salt concentration in the NLSB was analyzed. To simulate solute transport without considering the interaction and adsorption of solutes, the hydrodynamic dispersion coefficient was determined using the molecular diffusion coefficient D_d in free water and the longitudinal and transverse dispersivities, D_L and D_T, respectively, of the solutes.

At 25 °C, the diffusion coefficient of the solute was set to $D_d = 8.99 \times 10^{-5}$ m^2/d [44]. According to the empirical rule proposed by Gelhar [45], the longitudinal dispersivity is related to the research scale or the length of the seepage path. Schulze-Makuch [46] established the relationship between the longitudinal dispersivity of the solute and the characteristic length of the seepage path through numerous statistical analyses as follows:

$$D_L = 0.085 L_s^{0.81} \tag{5}$$

where L_s is the characteristic length of the seepage path. Bear [43] proposed that the transverse dispersivity is one-tenth the longitudinal dispersivity:

$$D_T = 0.1 D_L \tag{6}$$

For the LR, the selected solute longitudinal and transverse dispersivities are D_L = 1.03 m and D_T = 0.103 m, respectively.

2.5. Application Scenarios

2.5.1. Application in a Homogeneous Embankment

Reservoir R-01 was built in 1955 with a total storage capacity of 0.3 million m^3. It has a homogeneous earth embankment with a length of 97 m, a height of 9.5 m and a crest width of 4 m (Figure 6a). A site survey revealed several traces of termites in the embankment and vicinity of the reservoir, and leakage was observed on the downstream slope, which partially deformed the embankment. Some leakage was reportedly caused by *O. formosanus* (Shiraki).

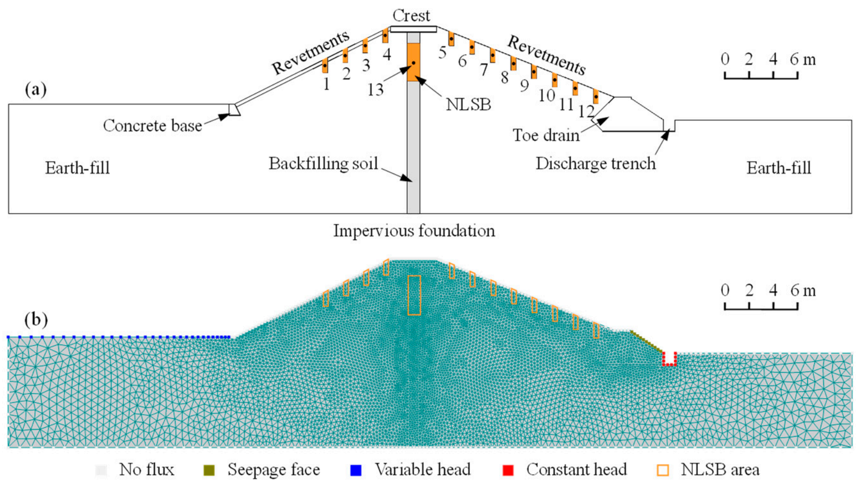

Figure 6. (**a**) Model geometry and (**b**) FEM mesh and boundary conditions of a homogeneous embankment (R-01). The positions of the observation points (1–13) are indicated by black dots.

As shown in Figure 6a, the embankment was backfilled by casing wells during the construction of the reinforcement. The casing wells were arranged in a single row along the embankment axis and revetments. They had a diameter of 1.1 m, and the compaction degree of the NLSB after backfilling was more than 0.96. The entire embankment section was backfilled with casing wells, and the bottom of the backfilling soil was 1.0 m below the relatively impervious foundation.

The calculation parameters and the initial and boundary conditions are consistent with those of the LR (Table 1 and Figure 6b). The revetments and concrete base are impervious, and the parameters of the backfilling soil are the same as those of the NLSB. Considering the solute transport simulation, the longitudinal dispersivity was determined to be 0.38 m using Equation (5), and the transverse dispersivity was set to 0.038 m. The normal water level of the reservoir was 4.04 m and the design flood level was 4.7 m. Considering the annual water level fluctuation, the variable head boundary was set as:

$$h(t) = \begin{cases} 2.04\,\text{m}, & 0 \le t < 60\,\text{d},\ 305\,\text{d} \le t \le 365\,\text{d} \\ 0.033\,t + 0.04\,\text{m}, & 60\,\text{d} \le t < 120\,\text{d} \\ 4.04\,\text{m}, & 120\,\text{d} \le t < 170\,\text{d},\ 195\,\text{d} \le t < 245\,\text{d} \\ 0.066\,t - 7.18\,\text{m}, & 170\,\text{d} \le t < 180\,\text{d} \\ 4.7\,\text{m}, & 180\,\text{d} \le t < 185\,\text{d} \\ -0.066\,t + 16.91\,\text{m}, & 185\,\text{d} \le t < 195\,\text{d} \\ -0.033\,t + 12.2\,\text{m}, & 245\,\text{d} \le t < 305\,\text{d} \end{cases} \tag{7}$$

The change in the reservoir water level is primarily affected by rainfall. As shown in Equation (7), the normal water level operation duration during the rainy season was set to 100 days and the design water flood operation duration was set to 5 days. The calculation assumes that the variable head cycle occurs 50 times and the total simulation time was 50 years.

2.5.2. Application in a Core-Wall Embankment

Reservoir R-02 was constructed between 1964 and 1979, with a total storage capacity of 0.31 million m^3. The main dam is made up of a core-wall embankment with a length of 131 m, height of 14.9 m and crest width of 5 m (Figure 7a). The reinforcement and the NLSB were the same as those applied to reservoir R-01. Furthermore, the calculation parameters and the boundary conditions used in the simulation were identical to those used for reservoir R-01 (Figure 7b). The longitudinal dispersivity was determined to be 0.56 m using Equation (5) and the transverse dispersivity was set to 0.056 m. The normal water level of the reservoir was 9.29 m and the design flood level was 10.25 m. Considering the annual water level fluctuation, the variable head boundary was set as:

$$h(t) = \begin{cases} 5.29\,\text{m}, & 0 \le t < 60\,\text{d},\ 305\,\text{d} \le t \le 365\,\text{d} \\ 0.066\,t + 1.29\,\text{m}, & 60\,\text{d} \le t < 120\,\text{d} \\ 9.29\,\text{m}, & 120\,\text{d} \le t < 170\,\text{d},\ 195\,\text{d} \le t < 245\,\text{d} \\ 0.096\,t - 7.03\,\text{m}, & 170\,\text{d} \le t < 180\,\text{d} \\ 10.25\,\text{m}, & 180\,\text{d} \le t < 185\,\text{d} \\ -0.096\,t + 28.01\,\text{m}, & 185\,\text{d} \le t < 195\,\text{d} \\ -0.066\,t + 25.62\,\text{m}, & 245\,\text{d} \le t < 305\,\text{d} \end{cases} \tag{8}$$

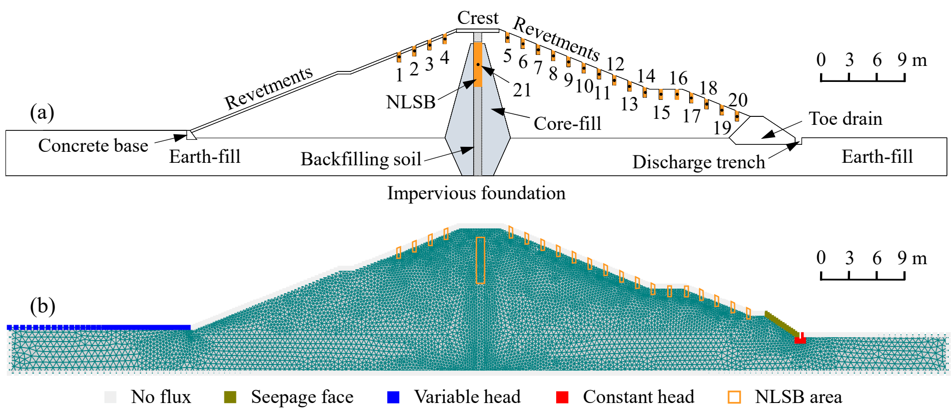

Figure 7. (**a**) Model geometry and (**b**) FEM mesh and boundary conditions for a core-wall embankment (R-02). The positions of the observation points (1–21) are indicated by black dots.

As in the case of reservoir R-01, the variable head cycle was assumed to occur 50 times and the total simulation time was 50 years.

3. Results and Discussion

3.1. NLSB Field Performance

Economic concerns. For the main dam of the LR, the direct cost of NLSBs was approximately 105,000 yuan, which was reduced by 30% to traditional termite control methods with termiticides. A survey of 20 reservoirs showed that the termite control cost used NLSBs was reduced by 25–35% compared with the traditional methods.

Environmental concerns. Because NLSB was designed to have low salt content (NaCl/soil ratio of 0.8%) and was located 1 m below the embankment outline, it has no obviously environmental impact on vegetation of the turf layer at the downstream slope. Even if a small amount of edible NaCl is leached, it will not affect the water quality of the reservoir and ensure the safety of drinking water in the water source. According to the NaCl-laden soil test, when the NaCl/soil ratio in treated soil is less than 3%, the physical properties of soil change marginally [47]. To our knowledge, no references have been found that suggest that NaCl is toxic to insect pests. However, the potential negative impact of NLSBs on the environment needs to be evaluated in the future.

Persistence and efficacy concerns. NLSBs have been used to control termites in the LR for 12 years, and no termite activity has been found through on-site inspection. The earliest commercial application of NLSB has been carried out in Zhejiang Province of China for more than 20 years and still shows resistance to termite attack. The persistence and efficacy of NLSBs still lack long-term observation and evaluation.

3.2. Simulated NaCl Concentration in the LR

The NaCl concentration in the LR at the end of the 1915-day simulation period is shown in Figure 8. The overall NaCl migration in the earth embankment was rather limited, especially above the phreatic line. According to a field survey, *O. formosanus* (Shiraki) nests in the earth embankment are generally located 1.5 m below the crest and above the phreatic line [24]. The phreatic line is an imaginary line separating the saturated zone and unsaturated zone in an earth embankment. Therefore, the NLSB can improve the core-fill of the dam above the phreatic line and provide long-term termite control.

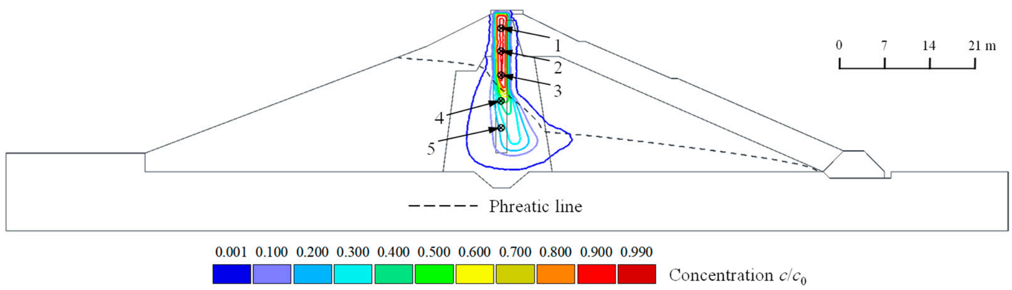

Figure 8. NaCl concentration isolines in the LR at the end of the 1915-day simulation. c_0 is the concentration of NaCl in the solid phase of the NLSB at the beginning of the simulation. The positions of the observation points (1–5) are indicated by crossed circles. The dashed line indicates the position of the phreatic line at the end of the 1915-day simulation.

Observation points were established at depths of 2.8 m, 6.3 m, 10 m, 13.9 m and 18 m from the embankment crest, along the central axis of the NLSB. The simulated and field-observed NaCl concentrations at the observation points during the simulation period are plotted in Figure 9. As shown, the NaCl concentrations above the phreatic line were clearly higher than those below the phreatic line. Although the number of observations is small, the simulated NaCl concentrations were close to the observed NaCl concentrations at the end of simulation period. The flow of the underground water below the phreatic line led to a rapid decrease in the NaCl concentrations at observation points 4 and 5, reducing them by 52% and 74%, respectively. In the following analyses of the application scenarios, the NLSB construction is above the phreatic line.

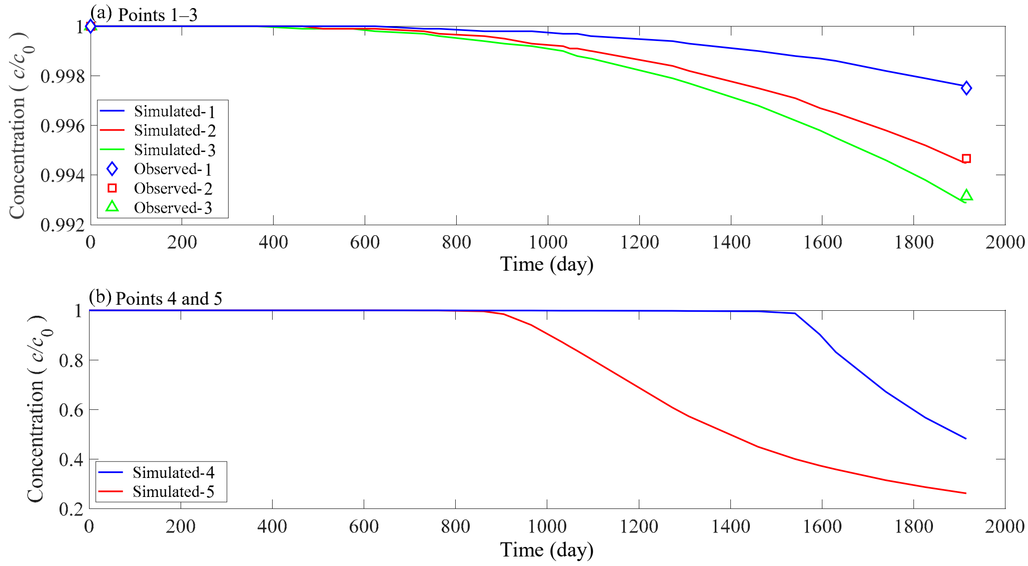

Figure 9. Simulated NaCl concentrations during the simulation period at observation points (**a**) 1–3 and (**b**) 4 and 5. The positions of the observation points (1–5) are indicated by crossed circles in Figure 8.

3.3. Barrier Longevity of the NLSB in Reservoir R-01

Figure 10 illustrates the temporal variation in the solute concentration at each observation point of the homogeneous embankment of reservoir R-01; the positions of the observation points are shown in Figure 6. As shown, the solute concentration at each observation point decreased significantly over time. At the end of the simulation period, the solute concentration at the point closest to the phreatic line decreased the most, from 8 g/kg to 0.45 g/kg, a decrease of 94%. The solute concentration at point 13, which is located at the backfilling center of the casing well, decreased the least, from 8 g/kg to 2.2 g/kg, a decrease of 73%. The decrease in solute concentration at points 5–12 on the downstream slope was essentially the same, with an average decrease of 81%.

The temporal variation in the cumulative solute mass in the homogeneous embankment is shown in Figure 11. During the simulation period, the cumulative flux of the solute (Figure 11a) outside the NLSB gradually increased to 111.2 kg/m, that of the solute in the NLSB (Figure 11b) and the total cross section (Figure 11c) gradually decreased by 82% and 6.6%, respectively, and that of solute transport and leaching (Figure 11d) gradually increased to 9.8 kg/m.

Hu et al. [48] proposed that NaCl-laden soil with a NaCl/soil ratio of 2 g/kg has resistance to termite attack. The areas with a concentration distribution of 2 g/kg at different times are shown in Figure 12a. When time = 10, 20, 30, 40 and 50 years, the total area with an NaCl concentration of 2 g/kg was 21.5, 16.7, 7.6, 4.4 and 2.6 m^2, respectively. The total initial area of the NLSB in the simulation area was 9.4 m^2, and the total area with a concentration of 2 g/kg was 9.5 m^2 at time = 27 years. Therefore, the protection range of the NLSB first increases and then decreases; after 27 years, the protection area is roughly the same as the initial area. When time = 30, 40 and 50 years, the protection range of the NLSB reduced by 19%, 53% and 72%, respectively.

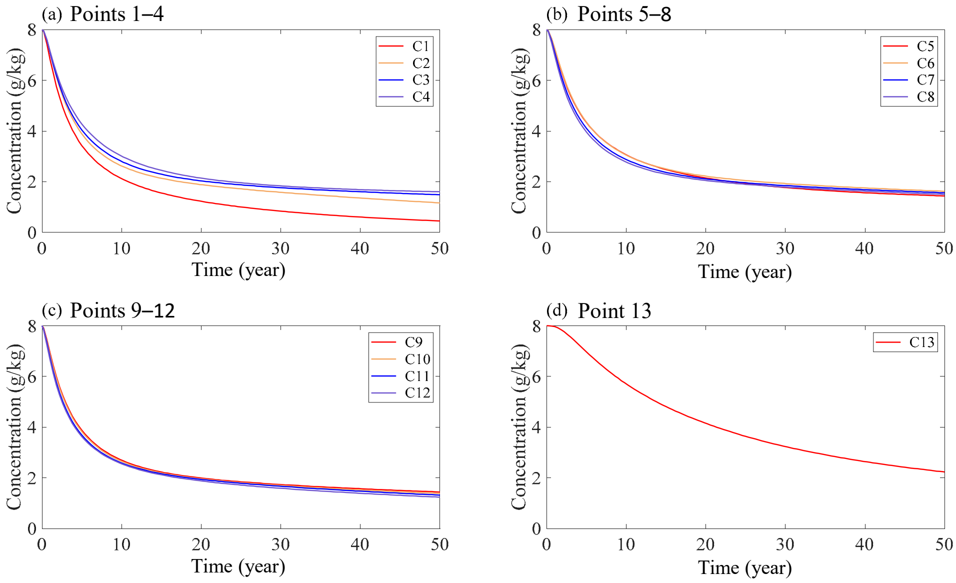

Figure 10. Simulated NaCl concentrations during the simulation period at observation points: (**a**) 1–4, (**b**) 5–8, (**c**) 9–12 and (**d**) 13 in reservoir R-01. The positions of the observation points 1–13 are indicated by black dots in Figure 6.

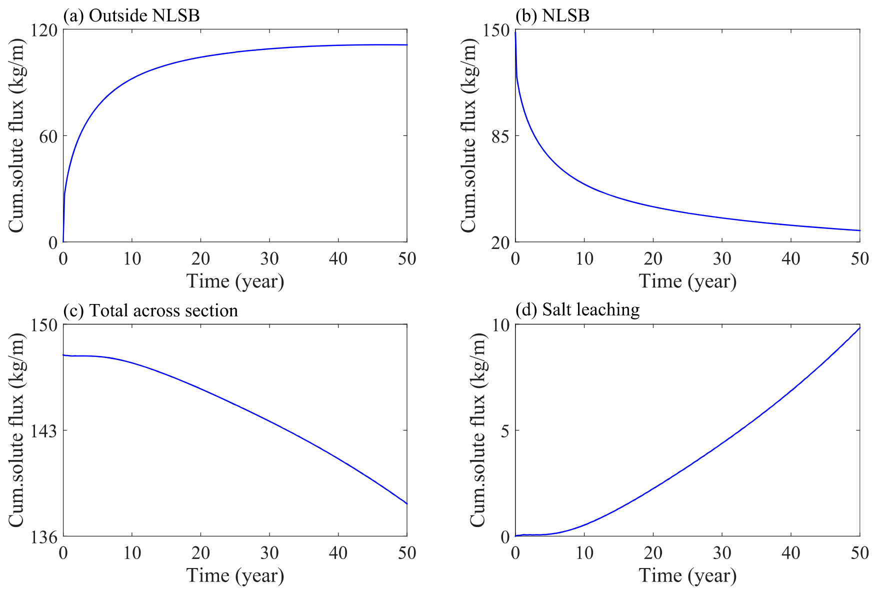

Figure 11. Temporal variation in cumulative solute mass in the study area: (**a**) outside the NLSB, (**b**) NLSB, (**c**) total cross section and (**d**) salt leaching of the homogeneous embankment.

Compared with the area near the slope surface, the salt desalination rate in the casing well backfilling area near the embankment axis was relatively gentle, and the salt loss of the upstream slope was faster than that of the downstream slope. Therefore, in the construction design of the NLSB, the initial salt concentration in different areas should be treated differently. The initial salt concentration ratios r_u and r_d of the upstream and downstream slopes, respectively, are defined as:

$$r_u = \frac{c_u}{c_a} \text{ and } r_d = \frac{c_d}{c_a}; \tag{9}$$

where c_u is the initial salt concentration in the upstream slope area (g/kg); c_d is the initial salt concentration in the downstream slope area (g/kg); c_a is the initial salt concentration in the dam axis area (g/kg). In general, r_u = 2.0–2.5 and r_d = 1.5–2.0.

Keeping all the other parameters unchanged, r_u = 2.0 and r_d = 1.5 were selected as an optimized design scheme. The areas with a calculated concentration distribution of 2 g/kg at various times are shown in Figure 12b. The results indicate that, with the optimized design scheme, when time = 10, 20, 30, 40 and 50 years, the area with a concentration distribution of 2 g/kg is 34.6 m^2, 34.3 m^2, 32.5 m^2, 29.1 m^2 and 24.2 m^2, respectively, exhibiting a gradually decreasing trend. However, at the end of the simulation period, the area with a concentration distribution of 2 g/kg increased by 157% compared to the initial total area of 9.4 m^2 in the simulation area. Therefore, the optimized design scheme provides a better termite control effect than the original one.

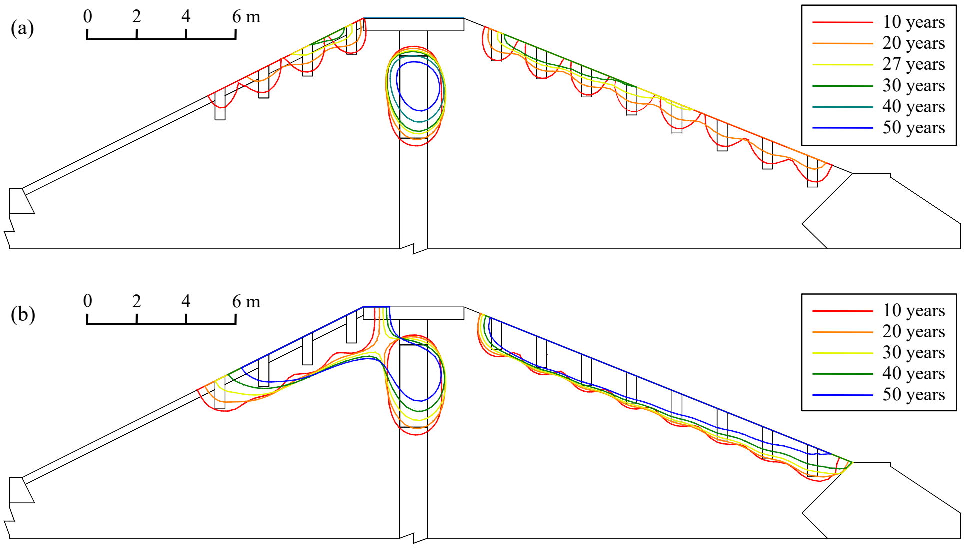

Figure 12. Areas with a concentration of 2 g/kg at various times in the homogeneous embankment with: (**a**) NaCl/soil ratio of 8 g/kg in the NLSB and (**b**) an optimized design scheme.

3.4. Barrier Longevity of the NLSB in Reservoir R-02

Figure 13 illustrates the temporal variation in the solute concentration at each observation point in the core-wall embankment of reservoir R-02; the positions of the observation points are shown in Figure 7. As shown, the solute concentration at each observation point decreased over time; however, the reduction was much smaller than that in the homogeneous dam. At the end of the simulation period, point 1 on the upstream slope closest to the phreatic line had the highest decrease in solute concentration, from 8 g/kg to 1.96 g/kg, a decrease of about 76%. The solute concentration at point 21, located at the backfilling center of the casing well, decreased the least, from 8 to 3.1 g/kg, a decrease of 61%. The decrease in solute concentration at points 5 to 20 on the downstream slope were essentially the same, with an average decrease of 70%.

The temporal variation in the cumulative solute mass in the study area of the core-wall embankment is shown in Figure 14. During the simulation period, the cumulative flux of the solute (Figure 14a) outside the NLSB gradually increased to 157.3 kg/m, that of the solute in the NLSB (Figure 14b) and the total cross section (Figure 14c) gradually decreased by 75% and 6.0%, respectively, and that of solute transport and leaching (Figure 14d) gradually increased to 13.8 kg/m.

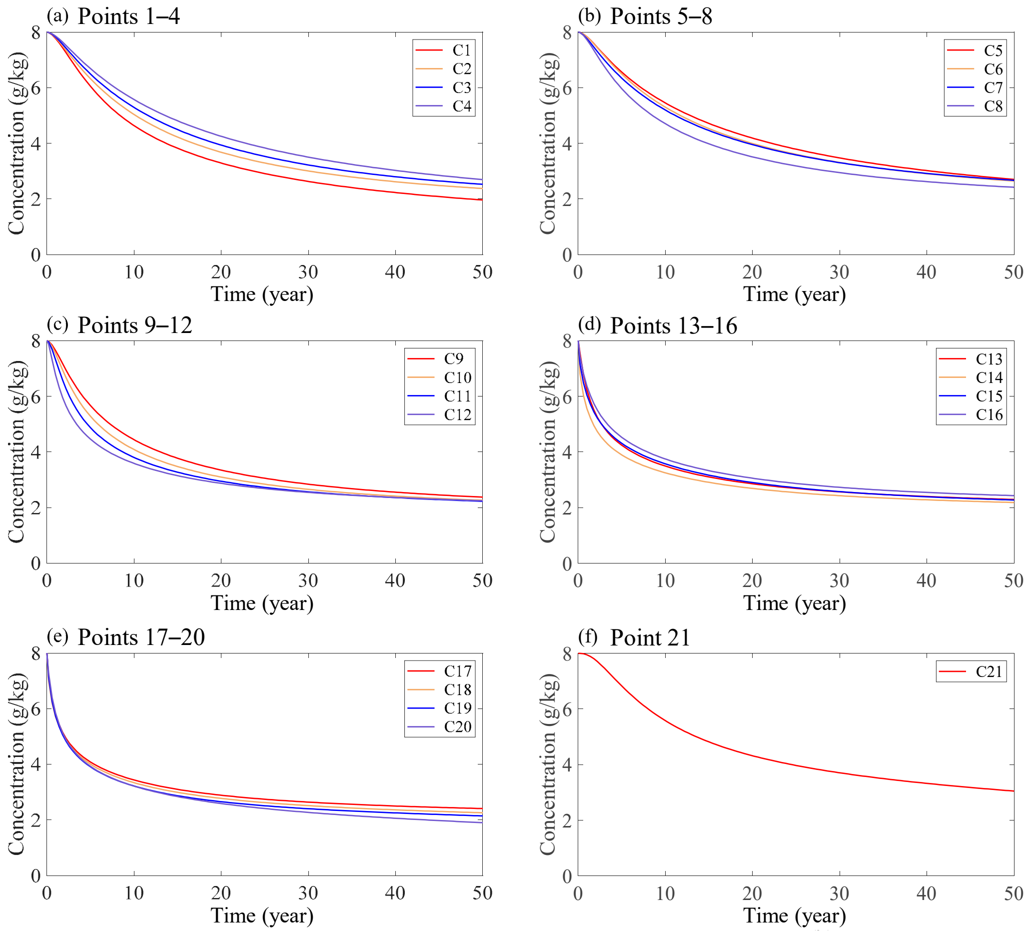

Figure 13. Temporal variation in NaCl concentration during the simulation period at observation points: (**a**) 1–4, (**b**) 5–8, (**c**) 9–12, (**d**) 13–16, (**e**) 17–20 and (**f**) 21 in reservoir R-02. The positions of the observation points (1–21) are indicated by black dots in Figure 7.

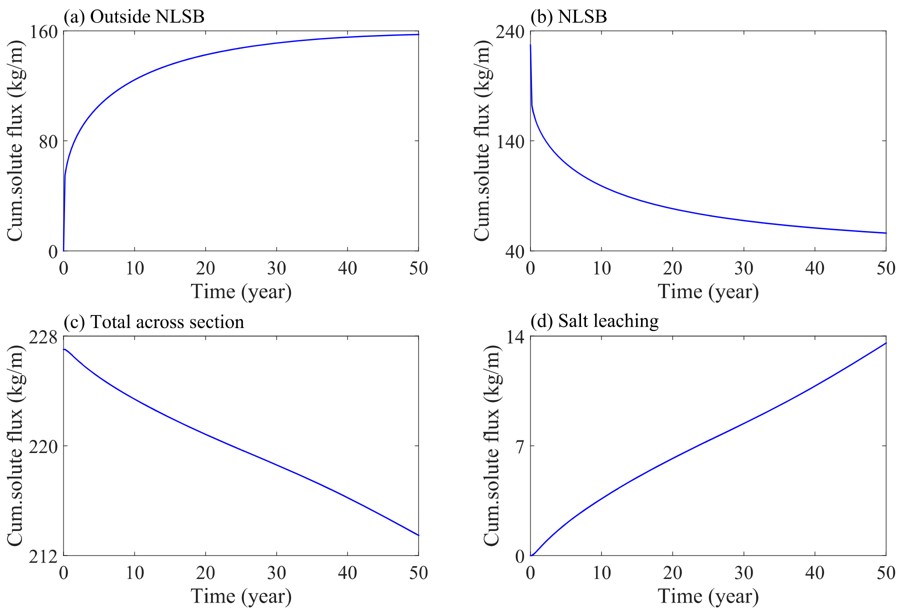

Figure 14. Temporal variation in cumulative solute mass in the study area: (**a**) outside the NLSB, (**b**) NLSB, (**c**) total cross section and (**d**) salt leaching of the core-wall embankment.

The solute concentration distribution in the simulated area at various times is shown in Figure 15. Initially, the total area of the NLSB in the simulation area was 14.4 m^2. When time = 10, 20, 30, 40 and 50 years, the area with a concentration of 2 g/kg was 39.2 m^2, 43.4 m^2, 45.1 m^2, 44.9 m^2 and 42.8 m^2, respectively, exhibiting an initial increasing trend followed by a decreasing trend. However, until the end of the simulation, the control effect of the NLSB still did not decrease significantly. Compared to the initial total area of the NLSB, the area with a concentration of 2 g/kg increased by 203% after 50 years. Despite the reduction in the total amount of solute in the NLSB over time due to advection and dispersion by moving water, the salt migration distance was relatively short and clustered around the NLSB, thereby maintaining the termite-preventive effect of the NLSB for more than 50 years.

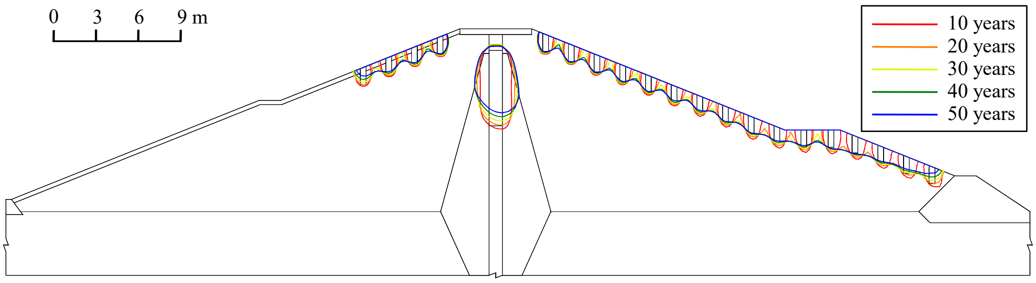

Figure 15. Areas with a concentration distribution of 2 g/kg at various times for a core-wall embankment.

4. Conclusions

NLSBs are a novel indigenous approach that uses NaCl-laden soil to build a barrier against subterranean termites. Although NLSBs are a sustainable alternative, limited scientific evaluation of their longevity has restricted their widespread adoption. Therefore, in this study, considering the LR and two types of reservoir dams in Zhejiang Province, we studied the long-term persistence of NLSBs using the HYDRUS (2D/3D) model, based on the extent of salt desalination.

The observed results showed that the low-cost NLSBs were environmentally friendly. No trace of termites has been found in the 12 years after the treatment of the LR. The simulated and observed NaCl concentrations were compared after a 1915-day simulation period, which revealed that the proposed simulation model performs well, and can effectively characterize salt migration from the NLSB.

Considering homogeneous dams, the salt desalination rate in the casing well backfill area near the embankment axis was relatively low, and the salt desalination rate of the upstream slope was higher than that of the downstream slope. Due to the diffusion of salt, the protection range of the NLSB first increased and then decreased. Based on the results, we recommend that, during the construction design of an NLSB, the initial salt concentrations ratios of the NLSB in the upstream and downstream slopes should be increased to 2.0 and 1.5, respectively. The protection area of the NLSB after 50 years increases by 157% compared to the initial area. The temporal decrease in the solute concentration in the NLSB of the core-wall embankment was significantly lesser than that of the homogeneous embankment. After 50 years, the termite control effect of the NLSB of the core-wall embankment did not decrease significantly.

The knowledge obtained through this research can be directly applied to the design and construction of agricultural embankments with anti-termite measures. In the future, in-depth studies should be undertaken to: (1) examine the sensitivity of the barrier longevity to the selected parameters, (2) develop an alternative three-dimensional model to improve the simulation accuracy, (3) perform long-term field tests for model calibration and (4) evaluate the potential negative impacts.

Author Contributions: Conceptualization, writing—original draft preparation, and funding acquisition, Y.L.; methodology, software, and formal analysis, Y.L. and D.-Z.P.; writing—review and editing, D.-Z.P. All authors have read and agreed to the published version of the manuscript.

Funding: This research was funded by the Public Welfare Technology Application Research Project of Zhejiang Province in China, grant number LGF19E090010.

Institutional Review Board Statement: Not applicable.

Informed Consent Statement: Not applicable.

Data Availability Statement: Not applicable.

Conflicts of Interest: The authors declare no conflict of interest.

References

1. Stephens, T. Manual on small earth dams: A guide to siting, design and construction. In *FAO Irrigation and Drainage Paper 64*; Food and Agriculture Organization of the United Nations: Rome, Italy, 2010.
2. Li, Y.; Dong, Z.Y.; Pan, D.Z.; Pan, C.H.; Chen, L.H. Effect of termite on soil pH and its application for termite control in Zhejiang Province, China. *Sociobiology* **2017**, *64*, 317–326. [CrossRef]
3. Zachariah, N.; Das, A.; Murthy, T.G.; Borges, R.M. Building mud castles: A perspective from brick-laying termites. *Sci. Rep.* **2017**, *7*, 4692. [CrossRef] [PubMed]
4. Li, G.X.; Dai, Z.R.; Yang, B. Introduction to termite research in China. *J. Appl. Entomol.* **1994**, *117*, 360–369.
5. Zhong, J.H.; Liu, L.L. Termite fauna in China and their economic importance. *Sociobiology* **2002**, *40*, 25–32.
6. Hu, J.; Zhong, J.H.; Guo, M.F. Alate dispersal distances of the black-winged subterranean termite Odontotermes formosanus (Isoptera: Termitidae) in southern China. *Sociobiology* **2007**, *50*, 1–8.
7. Wang, Z.; Guo, J.; Gong, Y.; Lu, W.; Lei, A. Control of dam termites with a monitor-controlling device (Isoptera: Termitidae). *Sociobiology* **2007**, *50*, 399–407.
8. Tian, W.J.; Ke, Y.L.; Zhuang, T.Y.; Wang, C.X.; Li, M.; Liu, R.Q.; Mao, W.G.; Zhang, S.S.; Li, D. Incipient colony development and biology of *Odontotermes formosanus* (Shiraki) and *O. hainanensis* (Light) (Isoptera: Termitidae). *J. Agric. Urban Entomol.* **2009**, *26*, 147–156. [CrossRef]
9. Hu, J.; Zhong, J.H.; Guo, M.F. Foraging territories of the black-winged subterranean termite *Odontotermes formosanus* (Isoptera: Termitidae) in southern China. *Sociobiology* **2006**, *48*, 1–12.
10. Market Supervisory Authority of Henan Province. *Technical Specification for Termite Control in Dikes and Dams, DB41/T 1761–2019*; Market Supervisory Authority of Henan Province: Zhengzhou, China, 2019.
11. Tuyen, V.V. Termite nest in dam site foundation before construction. In Proceedings of the Third Conference of Pacific Rim Termite Research Group, Guangzhou, China, 6–7 March 2006.
12. Tuyen, V.V. Termites in dikes of northern Vietnam. In *Pests of Forest Importance and Their Management*; Tyagi, B.K., Veer, V., Prakash, S., Eds.; New Delhi Scientific Publishers: New Delhi, India, 2014.
13. Henderson, G. The termite menace in New Orleans: Did they cause the floodwalls to tumble? *Am. Entomol.* **2008**, *54*, 156–162. [CrossRef]
14. Yang, X.; Henderson, G.; Mao, L.; Evans, A. Application of ground penetrating radar in detecting the hazards and risks of termites and ants in soil levees. *Environ. Entomol.* **2009**, *38*, 1241–1249. [CrossRef]
15. Hoon, R.C. The incidence of white ants (termites) in the region of the Hirakud Dam project. In *Proceedings of International Symposium on Termites in the Humid Tropic*; UNESCO: New Delhi, India, 1960.
16. Mahapatro, G.K.; Chatterjee, D. Termites as structural pest: Status in Indian scenario. *Proc. Natl. Acad. Sci. India Sect. B Biol. Sci.* **2017**, *88*, 977–994. [CrossRef]
17. Umaru, A.B.; Sangodoyin, A.Y.; Oke, I.A. On the causes and effects of earth dams failures in north-eastern Nigeria. *Int. J. Eng. Res. Technol.* **2014**, *3*, 2978–2985.
18. Shaleh, I.; Jannual, N.; Hasin, S.; Kaewgrajang, T.; Raffiudin, R.; Nipitwattanaphon, M. Identification of fungus-growing termites and mutualistic Termitomyces from two provinces in Thailand. *Int. J. Trop. Insect Sci.* **2020**, *41*, 1555–1566. [CrossRef]
19. Feng, K.; Lu, X.; Luo, J.; Tang, F. SMRT sequencing of the full-length transcriptome of Odontotermes formosanus (Shiraki) under Serratia marcescens treatment. *Sci. Rep.* **2020**, *10*, 15909. [CrossRef]
20. Ahmad, F.; Fouad, H.; Liang, S.-Y.; Hu, Y.; Mo, J.-C. Termites and Chinese agricultural system: Applications and advances in integrated termite management and chemical control. *Insect Sci.* **2021**, *28*, 2–20. [CrossRef] [PubMed]
21. Huang, F.-S.; Zhu, S.-M.; Ping, Z.-M.; He, X.-S.; Li, G.-X.; Gao, D.-R. *Fauna Sinica, Insecta, Vol. 17, Isoptera*; China Science Publishing: Beijing, China, 2000.
22. Acda, M.N. Sustainable termite management using physical barriers. In *Termites and Sustainable Management, Sustainability in Plant and Crop Protection*; Khan, M.A., Ahmad, W., Eds.; Springer International Publishing AG: Cham, Switzerland, 2018.
23. Chen, L.-H.; Pan, C.-H.; Chen, S.-M.; Song, X.-G.; Zheng, S.-Z.; Chen, S.-H. New technology of using salt to prevent termites for dikes and dams. *Chin. J. Geotech. Eng.* **2011**, *33*, 140–144.

24. Li, Y.; Pan, D.-Z. A simulation of salt transport in NaCl-laden soil barrier to control subterranean termites in an earth embankment. *Water* **2021**, *13*, 1204. [CrossRef]
25. Fagbohunka, B.S.; Edorh, S.E.; Adeyanju, M.M.; Ezima, E.N.; Alabi, M.A.; Ogunlabi, O.O. Activities of a cellulase of the termite, *Ametermes Eveuncifer* (Silverstri) soldier: Clue to termites salt intolerance. *J. Nat. Sci. Res.* **2015**, *5*, 117–123.
26. Hume, D.L. Termite Blocking System. U.S. Patent US005094028A, 10 March 1992.
27. Grace, K.J.; Yates, J.R.; Minoru, T.; Yamamoto, R.T. Persistence of organochlorine insecticides for Formosan subterranean termite (Isoptera: Rhinotermitidae) control in Hawaii. *J. Econ. Entomol.* **1993**, *86*, 761–766. [CrossRef]
28. Wei, D.; Kameya, T.; Urano, K. Environmental management of pesticidal POPs in China: Past, present and future. *Environ. Int.* **2007**, *33*, 894–902. [CrossRef]
29. Su, N.-Y. Technological needs for sustainable termite management. *Sociobiology* **2011**, *58*, 229–239.
30. Gold, R.E.; Howell, R.N.; Pawson, J.B.M.; Wright, M.S.; Luts, J.C. Persistence and termiticides to Subterranean termites (Isoptera: Rhinotermitidae) from five soil types and locations in Texas. *Sociobiology* **1996**, *28*, 337–363.
31. Wiltz, B.A.; Woodson, W.D.; Puterka, G.J. Potential of Kaolin-based particle film barriers for Formosan subterranean termite (Isoptera: Rhinotermitidae) control. *Sociobiology* **2010**, *55*, 405–413.
32. Alvarez-Benedi, J.; Munoz-Carpena, R. *Soil Water-Solute Process Characterization: An Integrated Approach*; CRC Press: London, UK, 2004.
33. Xu, J.; Wang, X.; Ding, Y.; Mu, Q.; Cai, H.; Ma, C.; Saddique, Q. Effects of irrigation and nitrogen fertilization management on crop yields and long-term dynamic characteristics of water and nitrogen transport at deep soil depths. *Soil Tillage Res.* **2020**, *198*, 104536. [CrossRef]
34. Rezaei, M.; Shahbazi, K.; Shahidi, R.; Davatgar, N.; Bazargan, K.; Rezaei, H.; Saadat, S.; Seuntjens, P.; Cornelis, W. How to relevantly characterize hydraulic properties of saline and sodic soils for water and solute transport simulations. *J. Hydrol.* **2021**, *598*, 125777. [CrossRef]
35. Simunek, J.; van Genuchten, M.T.; Sejna, M. Recent developments and applications of the HYDRUS computer software packages. *Vadose Zone J.* **2016**, *15*, 1–25. [CrossRef]
36. Salehi, A.A.; Navabian, M.; Varaki, M.E.; Pirmoradian, N. Evaluation of HYDRUS-2D model to simulate the loss of nitrate in subsurface controlled drainage in a physical model scale of paddy fields. *Paddy Water Environ.* **2017**, *15*, 433–442. [CrossRef]
37. Feng, F.; Zhang, Z.; Zhang, Z. Evaluating the sustainable use of saline water irrigation on soil water-salt content and grain yield under subsurface drainage condition. *Sustainability* **2019**, *11*, 6431. [CrossRef]
38. Chen, N.; Li, X.; Simunek, J.; Shi, H.; Hu, Q.; Zhang, Y. Evaluating soil nitrate dynamics in an intercropping dripped ecosystem using HYDRUS-2D. *Sci. Total Environ.* **2020**, *718*, 137314. [CrossRef]
39. Yadav, B.; Krishnan, P.; Shafeeq, P.M.; Parihar, C.M.; Aggarwal, P. Modelling soil thermal regime in wheat using HYDRUS-2D under diversified maize-wheat-mungbean cropping system. *Catena* **2020**, *194*, 104765. [CrossRef]
40. Defterdarovic, J.; Filipovic, L.; Kranjcec, F.; Ondrasek, G.; Kikic, D.; Novosel, A.; Mustac, I.; Krevh, V.; Magdic, I.; Rubinic, V.; et al. Determination of soil hydraulic parameters and evaluation of water dynamics and nitrate leaching in the unsaturated layered zone: A modeling case study in central Croatia. *Sustainability* **2021**, *13*, 6688. [CrossRef]
41. Simunek, J.; van Genuchten, M.T.; Sejna, M. The HYDRUS Software Package for Simulating Two-and Three Dimensional Movement of Water, Heat, and Multiple Solutes in Variably-Saturated Porous Media. In *Technical Manual, Version 2.0*; PC Progress: Prague, Czech Republic, 2012.
42. van Genuchten, M.T. A closed-form equation for predicting the hydraulic conductivity of unsaturated soils. *Soil Sci. Soc. Am. J.* **1980**, *44*, 892–898. [CrossRef]
43. Bear, J. *Dynamics of Fluid in Porous Media*; Elsevier: New York, NY, USA, 1972.
44. Rowe, R.K.; Badv, K. Advective-Diffusive contaminant migration in unsaturated sand and gravel. *J. Geotech. Eng.* **1996**, *122*, 965–975. [CrossRef]
45. Gelhar, L.W. *Stochastic Subsurface Hydrology*; Prentice-Hall: Englewood Cliffs, NJ, USA, 1993.
46. Schulze-Makuch, D. Longitudinal dispersivity data and implications for scaling behavior. *Ground Water* **2005**, *43*, 443–456. [CrossRef] [PubMed]
47. Chen, S.; Shen, S.; Chen, L.; Lu, G. Test of engineering properties of impervious soil with salt. *Adv. Sci. Technol. Water Resour.* **2015**, *35*, 66–70.
48. Hu, Y.; Song, X.-G.; Chen, L.-H.; Ruan, G.-H.; Zhou, Y.-Q. Effect of saline soil in controlling termites. *Chin. J. Vector. Biol. Control* **2014**, *25*, 148–151.